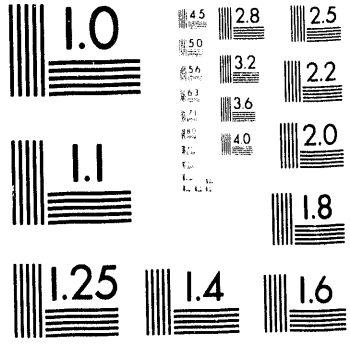
1.0
1.1
1.25
1.4
1.6
1.8
2.0
2.2
2.5
2.8
3.2
3.6
4.0
4.5
5.0

1 of 1

Vehicle/Guideway Interaction and Ride Comfort in Maglev Systems*

by

Y. Cai, S. S. Chen, D. M. Rote and H. T. Coffey
Argonne National Laboratory
Argonne, IL 60439

For presentation at the International Conference on Speedup Technology for Railway and Maglev Vehicles, November 22-26, 1993, Yokohama, Japan; Submitted to ASME J. Dynamic System, Measurement and Control.

*Work performed under the sponsorship of the U.S. Army Corps of Engineers and the Federal Railroad Administration through interagency agreements with the U.S. Department of Energy.

Vehicle/Guideway Interaction and Ride Comfort in Maglev Systems

by

Y. Cai, S. S. Chen, D. M. Rote and H. T. Coffey
Argonne National Laboratory
Argonne, IL 60439

ABSTRACT

The importance of vehicle/guideway dynamics in maglev systems is discussed. The particular interests associated with modeling vehicle/guideway interactions and explaining response characteristics of maglev systems for a multicar, multiload vehicle traversing on a single- or double-span flexible guideway are considered, with an emphasis on vehicle/guideway coupling effects, comparison of concentrated and distributed loads, and ride comfort. Coupled effects of vehicle/guideway interactions over a wide range of vehicle speeds with various vehicle and guideway parameters are investigated, and appropriate criteria for decoupling at critical vehicle speeds or crossing frequencies are identified.

INTRODUCTION

A high-speed ground transportation system, based on maglev vehicles propelled by a linear electric motor, has been proposed to meet future intercity transportation requirements. One possible and attractive approach is replacement of air travel for selected intercity trips of 150 to 1000 km. The maglev system will offer the advantages of lower noise and emissions and better ride quality, as well as potential energy savings and economic benefits, relative to conventional rail systems (1-6).

While some maglev design concepts have been developed nearly to commercial application, the attractiveness of maglev systems is expected to be enhanced even further over the next several years by new or improved concepts, improved design and construction methods, and new material (including high-temperature superconductors, high-energy permanent magnets, and advanced material for guideways). It is therefore reasonable to expect that maglev systems may indeed be a key transportation mode in the 21st century (2).

For several decades, research and development have been performed in the areas of magnetic levitation, response of maglev vehicles to rough guideways, interaction of variously suspended vehicles with flexible guideways, and optimization of vehicle suspensions. The results of these efforts are useful in providing appropriate criteria for the design of maglev systems (1,5,7-9).

The dynamic response of magnetically levitated vehicles is important because of safety, ride quality, guideway design, and system cost. More emphasis should be placed on guideway design, because the cost of the guideway structure is expected to be 60-80% of the overall initial capital investment cost (6,10). Thus, guideway design is a critical area of potential capital savings. More-flexible guideways are less expensive, but cause complex vehicle/guideway interactions and affect ride quality. An optimized guideway design will be important for a high-speed maglev system that offers good ride quality. As maglev vehicle speeds increase to 300-500 km/h, or as guideways become lighter and more flexible to reduce costs, the dynamic interactions between vehicle and guideway become an important problem and will play a dominant role in establishing vehicle suspension requirements and specifications for guideway stiffness, weight, and span length (6,7,11-16).

Light guideways, especially those made of steel, may be susceptible to dynamic instability and unacceptable vibration, and thus dynamic evaluation must be included in the structural analysis. Different dynamic responses of coupled vehicle/guideway systems may be observed, including periodic oscillation, random vibration, dynamic instability, chaotic motion, parametric resonance, combination resonance, and transient response (2).

To design a proper guideway that provides acceptable ride quality, the dynamic interaction of vehicles and guideways must be understood. Furthermore, the trade-off between guideway smoothness and design of the levitation and control systems must be considered if the maglev system is to be economically feasible. The coupled vehicle/guideway dynamics are the link between the guideway and the other maglev components. Thus, reliable analytical and simulation techniques are needed in the design of vehicle/guideway systems (2,11-14,16). Furthermore, a coupled vehicle/guideway dynamic model with multiple cars and multiple loads must be developed to meet system design requirements. This analytical model should also be easily incorporated into the computer code for dynamic simulation of maglev systems (11-14).

Therefore, this study is focused on the dynamics of maglev vehicles and guideways. We discuss the problems associated with modeling vehicle/guideway interactions and then explain the response characteristics of maglev systems for a multicar, multiload vehicle traveling on a single- or double-span flexible guideway, with emphasis on vehicle/guideway coupling effects, comparison of concentrated and distributed loads, and ride comfort (13).

EQUATIONS OF MOTION

The Vehicle Model

A multicar, multiload vehicle traveling along a flexible guideway at a velocity v, as shown in Fig. 1, is considered in our mathematical model for dynamic analysis of vehicle/guideway interactions. The car body is rigid and has a uniform mass. The center of mass is consistent with that of the moment of inertia. Each car is supported by magnets (or bogies) with linear springs and dampings (see Fig. 2), which form the primary and secondary suspensions of the vehicle. If there is only one magnet (i.e., the unsprung mass) attached to the vehicle, there is a single concentrated load and only one-dimensional motion (i.e., heave motion) of the vehicle. If there are multiple magnets on the vehicle, the loads are considered multiple or distributed and the vehicle is capable of both heave and pitch motions. In this study, only vertical vehicle motion is considered because it is dominant in the dynamic analysis of vehicle/guideway interactions.

The equations of motion for the vehicle are then

$$m_s\ddot{y}_{si} + c_s\sum_{j=1}^{N}\left(\dot{y}_{si} - \dot{y}_{pij}\right) + k_s\sum_{j=1}^{N}\left(y_{si} - y_{pij}\right) + c_v\left\{\left[\dot{y}_{si} - \dot{y}_{s(i-1)}\right] + \left[\dot{y}_{si} - \dot{y}_{s(i+1)}\right]\right\} + k_v\left\{\left[y_{si} - y_{s(i-1)}\right] + \left[y_{si} - y_{s(i+1)}\right]\right\} = -m_s g \quad (1)$$

$$(i = 2, \ldots, M-1; \quad j = 1, \ldots, N)$$

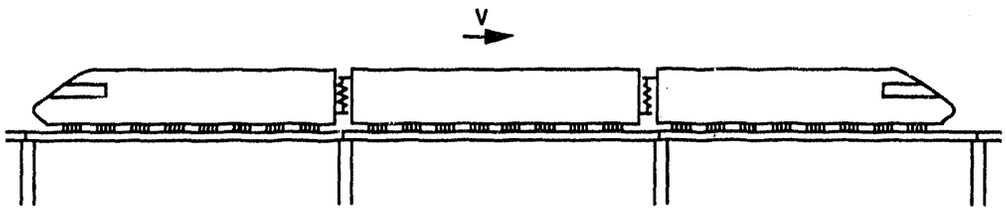

Fig. 1 Model of multicar, multiload maglev vehicle traveling along a guideway

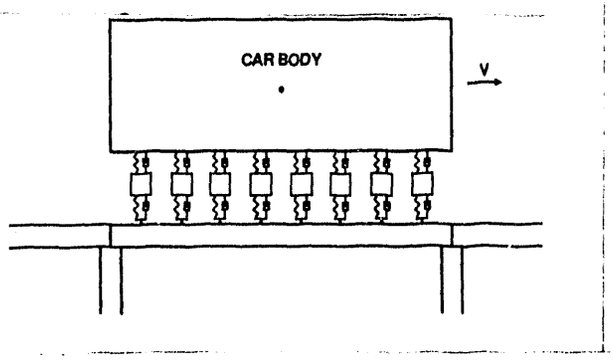

Fig. 2 Model of single car supported with multiple magnets and traveling along a guideway

$$m_s\ddot{y}_{s1} + c_s\sum_{j=1}^{N}\left(\dot{y}_{s1} - \dot{y}_{p1j}\right) + k_s\sum_{j=1}^{N}\left(y_{s1} - y_{p1j}\right) + c_v\left(\dot{y}_{s1} - \dot{y}_{s2}\right) + k_v\left(y_{s1} - y_{s2}\right) = -m_s g \qquad (i = 1;\ \ j = 1, ..., N) \tag{2}$$

$$m_s\ddot{y}_{sM} + c_s\sum_{j=1}^{N}\left(\dot{y}_{sM} - \dot{y}_{pMj}\right) + k_s\sum_{j=1}^{N}\left(y_{sM} - y_{pMj}\right) + c_v\left[\dot{y}_{sM} - \dot{y}_{s(M-1)}\right] + k_v\left[y_{sM} - y_{s(M-1)}\right] = -m_s g \qquad (i = M;\ \ j = 1, ..., N) \tag{3}$$

and

$$m_p\ddot{y}_{pij} + c_p\left(\dot{y}_{pij} + \dot{y}_{gij}\right) + k_p\left(y_{pij} + y_{gij}\right) - c_s\left(\dot{y}_{si} - \dot{y}_{pij}\right) - k_s\left(y_{si} - y_{pij}\right) = -m_p g \qquad (i = 1, ..., M;\ \ j = 1, ..., N) \tag{4}$$

where lumped masses m_p and m_s, linear springs k_p and k_s, and dampings c_p and c_s represent primary and secondary suspensions; the displacement of two suspensions are y_p and y_s; subscript i represents i-th car body and subscript j represents j-th magnet on the i-th car; M is number of cars; N is number of magnets on each car; and k_v and c_v are intercar stiffness and damping, representing constraints between adjacent cars. For a magnetic primary suspension, k_p and c_p represent magnetic gap stiffness and passive damping. y_{gij} is guideway displacement input at the i-th car and the j-th magnet.

Uncoupled natural frequencies and modal damping ratios are defined as

$$\omega_p = \sqrt{\frac{k_p}{m_p}},\quad \zeta_p = \frac{c_p}{2m_p\omega_p},\quad \omega_s = \sqrt{\frac{Nk_s}{m_s}},\quad \zeta_s = \frac{Nc_s}{2m_s\omega_s}. \tag{5}$$

And several nondimensional parameters are introduced:

$$\alpha_c = \frac{c_v}{c_s},\quad \alpha_k = \frac{k_v}{c_s},\quad \beta_c = \frac{c_s}{c_p},\quad \beta_k = \frac{k_s}{k_p}. \tag{6}$$

Using Eqs. 5 and 6, we can rewrite Eqs. 1-4 as

$$\ddot{y}_{si} + 2\zeta_s\omega_s\dot{y}_{si} - 2\zeta_s\omega_s/N\sum_{j=1}^{N}\dot{y}_{pij} + \omega_s^2 y_{si} - \omega_s^2/N\sum_{j=1}^{N}y_{pij} + 2\zeta_s\omega_s\alpha_c\left[2\dot{y}_{si} - \dot{y}_{s(i-1)} - \dot{y}_{(i+1)}\right] + \omega_s^2\alpha_k\left[2y_{si} - y_{s(i-1)} - y_{s(i+1)}\right] = -g \qquad (i = 2, ..., M-1;\ j = 1, ..., N) \tag{7}$$

$$\ddot{y}_{s1} + 2\zeta_s\omega_s\dot{y}_{s1} - 2\zeta_s\omega_s/N\sum_{j=1}^{N}\dot{y}_{p1j} + \omega_s^2 y_{s1} - \omega_s^2/N\sum_{j=1}^{N}y_{p1j} + 2\zeta_s\omega_s\alpha_c\left(\dot{y}_{s1} - \dot{y}_{s2}\right) + \omega_s^2\alpha_k\left(y_{s1} - y_{s2}\right) = -g \qquad (i = 1;\ j = 1, ..., N) \tag{8}$$

$$\ddot{y}_{sM} + 2\zeta_s\omega_s\dot{y}_{sM} - 2\zeta_s\omega_s/N\sum_{j=1}^{N}\dot{y}_{pMj} + \omega_s^2 y_{sM} - \omega_s^2/N\sum_{j=1}^{N}y_{pMj} + 2\zeta_s\omega_s\alpha_c\left[\dot{y}_{sM} - \dot{y}_{s(M-1)}\right] + \omega_s^2\alpha_k\left[y_{sM} - y_{s(M-1)}\right] = -g \qquad (i = M;\ j = 1, ..., N) \tag{9}$$

and

$$\ddot{y}_{pij} + 2\zeta_p\omega_p(1+\beta_c)\dot{y}_{pij} + \omega_p^2(1+\beta_k)y_{pij} - 2\zeta_p\omega_p\beta_c\dot{y}_{si} - \omega_p^2\beta_k y_{si} = -g - 2\zeta_p\omega_p\dot{y}_{gij} - \omega_p^2 y_{gij} \qquad (i = 1, ..., M;\ j = 1, ..., N). \tag{10}$$

The system of Eqs. 7-10 can be represented in matrix form by an M + M × N size set:

$$\mathbf{M}\ddot{\mathbf{y}} + \mathbf{C}\dot{\mathbf{y}} + \mathbf{K}\mathbf{y} = \mathbf{Q} \tag{11}$$

where

$$\mathbf{y} = \begin{bmatrix} \mathbf{y}_1 \\ \mathbf{y}_2 \end{bmatrix},$$

$$\mathbf{y}_1 = \begin{bmatrix} y_{s1} \\ y_{s2} \\ \vdots \\ y_{sM} \end{bmatrix}_{M\times 1},\qquad \mathbf{y}_2 = \begin{bmatrix} y_{p11} \\ y_{p12} \\ y_{p1N} \\ \vdots \\ y_{pM1} \\ y_{pM2} \\ \vdots \\ y_{pMN} \end{bmatrix}_{(M\,N)\times 1}, \tag{12}$$

$$\mathbf{Q} = \begin{bmatrix} \mathbf{Q}_1 \\ \hline \mathbf{Q}_2 \end{bmatrix},$$

$$\mathbf{Q}_1 = \begin{bmatrix} -g \\ -g \\ \vdots \\ -g \end{bmatrix}_{M\times 1}, \qquad \mathbf{Q}_2 = \begin{bmatrix} -g - 2\zeta_p\omega_p\dot{y}_{g11} - \omega_p^2 y_{g11} \\ -g - 2\zeta_p\omega_p\dot{y}_{g12} - \omega_p^2 y_{g12} \\ \vdots \\ -g - 2\zeta_p\omega_p\dot{y}_{g1N} - \omega_p^2 y_{g1N} \\ \vdots \\ -g - 2\zeta_p\omega_p\dot{y}_{gM1} - \omega_p^2 y_{gM1} \\ -g - 2\zeta_p\omega_p\dot{y}_{gM2} - \omega_p^2 y_{gM2} \\ \vdots \\ -g - 2\zeta_p\omega_p\dot{y}_{gMN} - \omega_p^2 y_{gMN} \end{bmatrix}_{(M\cdot N)\times 1},$$

$$\mathbf{M} = \begin{bmatrix} 1 & & & \\ & 1 & & 0 \\ & & \ddots & \\ & 0 & & 1 \end{bmatrix}_{(M+M\cdot N)\times(M+M\cdot N)}, \qquad (12)$$

$$\mathbf{C} = \left[\begin{array}{c|c} \mathbf{C}_{11} & \mathbf{C}_{12} \\ \hline \mathbf{C}_{21} & \mathbf{C}_{22} \end{array}\right]_{(M+M\cdot N)\times(M+M\cdot N)}, \qquad \text{(Contd.)}$$

$$\mathbf{C}_{11} = \begin{bmatrix} 2\zeta_s\omega_s(1+\alpha_c) & -2\zeta_s\omega_s\alpha_c & 0 & 0 & \cdots \\ -2\zeta_s\omega_s\alpha_c & 2\zeta_s\omega_s(1+2\alpha_c) & -2\zeta_s\omega_s\alpha_c & 0 & \cdots \\ 0 & -2\zeta_s\omega_s\alpha_c & 2\zeta_s\omega_s(1+2\alpha_c) & -2\zeta_s\omega_s\alpha_c & \cdots \\ \vdots & \vdots & \vdots & \vdots & \vdots \end{bmatrix}_{M\times M},$$

$$\mathbf{C}_{12} = \begin{bmatrix} -2\zeta_s\omega_s/N & \cdots & -2\zeta_s\omega_s/N & 0 & \cdots & 0 & \cdots \\ 0 & \cdots\cdots & 0 & -2\zeta_s\omega_s/N & \cdots & -2\zeta_s\omega_s/N & \cdots \\ \vdots & \vdots & \vdots & \vdots & \vdots & \vdots & \vdots \end{bmatrix}_{M\times(M\cdot N)},$$

$$\mathbf{C}_{21} = \begin{bmatrix} -2\zeta_p\omega_p\beta_c & 0 & \cdots \\ \vdots & \vdots & \cdots \\ -2\zeta_p\omega_p\beta_c & 0 & \cdots \\ 0 & -2\zeta_p\omega_p\beta_c & \cdots \\ \vdots & \vdots & \cdots \\ 0 & -2\zeta_p\omega_p\beta_c & \cdots \\ \vdots & \vdots & \vdots \end{bmatrix}_{(M\cdot N)\times M},$$

$$\mathbf{C}_{22} = \begin{bmatrix} 2\zeta_p\omega_p(1+\beta_c) & 0 & 0 & \cdots \\ 0 & 2\zeta_p\omega_p(1+\beta_c) & 0 & \cdots \\ 0 & 0 & 2\zeta_p\omega_p(1+\beta_c) & \cdots \\ \vdots & \vdots & \vdots & \vdots \end{bmatrix}_{(M\cdot N)\times(M\cdot N)},$$

$$\mathbf{K} = \left[\begin{array}{c|c} \mathbf{K}_{11} & \mathbf{K}_{12} \\ \hline \mathbf{K}_{21} & \mathbf{K}_{22} \end{array}\right],$$

$$\mathbf{K}_{11} = \begin{bmatrix} \omega_s^2(1+\alpha_k) & -\omega_s^2\alpha_k & 0 & 0 & \cdots \\ -\omega_s^2\alpha_k & \omega_s^2(1+2\alpha_k) & -\omega_s^2\alpha_k & 0 & \cdots \\ 0 & -\omega_s^2\alpha_k & \omega_s^2(1+2\alpha_k) & -\omega_s^2\alpha_k & \cdots \\ \vdots & \vdots & \vdots & \vdots & \vdots \end{bmatrix}_{M\times M},$$

$$\mathbf{K}_{12} = \begin{bmatrix} -\omega_s^2/N & \cdots & -\omega_s^2/N & 0 & \cdots & 0 & \cdots \\ 0 & \cdots\cdots & 0 & -\omega_s^2/N & \cdots & -\omega_s^2/N & \cdots \\ \vdots & \vdots & \vdots & \vdots & \vdots & \vdots & \vdots \end{bmatrix}_{M\times(M\cdot N)},$$

$$\mathbf{K}_{21} = \begin{bmatrix} -2\omega_p^2\beta_k & 0 & \cdots \\ \vdots & \vdots & \cdots \\ -2\omega_p^2\beta_k & 0 & \cdots \\ 0 & -2\omega_p^2\beta_k & \cdots \\ \vdots & \vdots & \cdots \\ 0 & -2\omega_p^2\beta_k & \cdots \\ \vdots & \vdots & \vdots \end{bmatrix}_{(M\cdot N)\times M},$$

$$\mathbf{K}_{22} = \begin{bmatrix} \omega_p^2(1+\beta_k) & 0 & 0 & \cdots \\ 0 & \omega_p^2(1+\beta_k) & 0 & \cdots \\ 0 & 0 & \omega_p^2(1+\beta_k) & \cdots \\ \vdots & \vdots & \vdots & \vdots \end{bmatrix}_{(M\cdot N)\times(M\cdot N)}. \qquad (12)$$

(Contd.)

If M = 1 and N = 1, the system of Eqs. 11 and 12 will represent the vehicle to be a one-dimensional model with two degrees of freedom (11-13).

The Guideway Model

For typical guideway systems, span-length-to-width ratios are large enough so that individual spans may be considered as beams rather than as plates. Thus, a Bernoulli-Euler beam model can be applied to a freely supported, homogeneous, isotropic, and uniform-cross-section guideway.

The equations of motion for guideway spans carrying a multicar, multiload vehicle may be derived as

$$EI\frac{\partial^4 y_k}{\partial x^4} + C\frac{\partial y_k}{\partial t} + m\frac{\partial^2 y_k}{\partial t^2} = F_k(x,t), \qquad (13)$$

where x is the axial coordinate of the beams, t is time, EI is the bending rigidity of the beams, C is the viscous damping coefficient (where we assume damping in a span is linear, viscous damping), and m is the beam mass per unit length. y_k is displacement of the k-th beam where the vehicle is traveling. $F_k(x,t)$ is the exciting force of the k-th beam due to the multicar, multiload vehicle acting on the beam,

$$F_k(x,t) = \sum_{k_i=1}^{n_k} f_{k_i}(t)\,\delta\left(x_{k_i} - vt\right), \qquad (14)$$

$$f_{k_i}(t) = -\left[c_p\left(\dot{y}_{pij} - \dot{y}_{k_i}\right) + k_p\left(y_{pij} - y_{k_i}\right)\right], \qquad (15)$$

where y_{pij} is the displacement of primary suspension of i-th car and j-th magnet on the k-th beam, y_{k_j} is the displacement of k-th beam on the point k_j corresponding to the displacement y_{pij}, and n_k is the total number of forces applied to the k-th beam by the vehicle.

For simply supported beams, the boundary conditions of the k-th beam are

$$y_k(t,0) = \frac{\partial^2 y_k(t,0)}{\partial x^2} = 0, \qquad y_k(t,L) = \frac{\partial^2 y(t,L)}{\partial x^2} = 0. \qquad (16)$$

If there is a double-span beam (total length is 2L), the slope and bending moment at an interior simple support must be continuous (11-13); thus

$$\begin{aligned} y_k(t,x)\big|_{x\to L-} &= y_k(t,x)\big|_{x\to L+} = 0, \\ \frac{\partial y_k(t,x)}{\partial x}\bigg|_{x\to L-} &= \frac{\partial y_k(t,x)}{\partial x}\bigg|_{x\to L+}, \\ \frac{\partial^2 y_k(t,x)}{\partial x}\bigg|_{x\to L-} &= -\frac{\partial^2 y_k(t,x)}{\partial x}\bigg|_{x\to L+}, \end{aligned} \qquad (17)$$

and there are

$$y_k(t,2L) = \frac{\partial^2 y(t,2L)}{\partial x^2} = 0. \tag{18}$$

The initial conditions are

$$y_k(x,0) = \frac{\partial y_k(x,0)}{\partial t} = 0. \tag{19}$$

In the modal analysis method, displacement of the beam is expressed as

$$y_k(x,t) = \sum_{n=1}^{\infty} q_{kn}(t)\varphi_n(x), \tag{20}$$

where $q_{kn}(t)$ are time-varying modal amplitudes and $\varphi_n(x)$ are modal shape functions that are orthogonal over the beam length $0 < x < L$. For a single-span beam,

$$\varphi_n(x) = \sqrt{2}\sin\left(\frac{n\pi x}{L}\right) = \sqrt{2}\sin\left(\lambda_n \frac{x}{L}\right), \qquad n = 1,2,3,\ldots; \tag{21}$$

for a double-span beam

$$\varphi_n(x) = \sin\left[\frac{(n+1)\pi}{2}\frac{x}{L}\right] = \sin\left(\lambda_n \frac{x}{L}\right), \qquad n = 1,3,5,7,9,\ \ldots, \tag{22}$$

$$\left.\begin{aligned} \varphi_n(x) &= \sin\lambda_n\frac{x}{L} - \frac{\sin\lambda_n}{\sinh\lambda_n}\sinh\lambda_n\frac{x}{L} \qquad 0 \le x \le L \\ \varphi_n(x) &= \sin\lambda_n\left(\frac{2L-x}{L}\right) - \frac{\sin\lambda_n}{\sinh\lambda_n}\sinh\lambda_n\left(\frac{2L-x}{L}\right) \qquad L \le x \le 2L \end{aligned}\right\} n = 2,4,6,8,10,\ldots, \tag{23}$$

where λ_n in Eq. 23 (eigenvalue of the n-th mode for double-span beam vibration) is the solution of the characteristic equation

$$\tan\lambda_n = \tanh\lambda_n. \tag{24}$$

The values of λ_n obtained from Eq. 24 are 3.39, 7.07, 10.21, 13.35, ...

$q_{kn}(t)$ is the solution of the equations

$$\frac{d^2 q_{kn}}{dt^2} + 2\zeta_n\omega_n\frac{dq_{kn}}{dt} + \omega_n^2 q_{kn} = \frac{1}{Lm}\int_0^L F_k(x,t)\varphi_n(x)dx, \tag{25}$$

where ω_n and ζ_n (the circular frequency and modal damping ratio of the beams) are given by

$$\omega_n = \frac{\lambda_n^2}{L^2}\sqrt{\frac{EI}{m}}, \qquad \zeta_n = \frac{C}{2m\omega_n}. \tag{26}$$

NUMERICAL SIMULATIONS

Numerical simulations of dynamic interactions of vehicle/guideway systems, schematically shown in Figs. 1 and 2, were carried out on the basis of the governing equations for the vehicle and guideway. Because of the coupled dynamic interaction between the vehicle and guideway (as indicated in Eq. 10 where guideway deflections are input to the vehicle, and in Eq. 15 where vehicle static weight and acceleration forces are excitations to the guideway), an iterated method is required in numerical simulations to calculate dynamic response of both vehicle and guideway, when the fourth-order Runge-Kutta method is applied in the simulations. For maglev vehicles restricted to vertical accelerations of <0.05 g, the inertia force is much lower than the static load, and dynamic coupling will be weak (16). In this case, the iteration is not needed. Because the integrating time-step is small enough, deflections of guideway spans in the previous time-step can be used as input to the vehicle, and dynamic responses of the vehicle can then be calculated and the results used to calculate guideway response at the current time-step. This calculating sequence proved efficient when coupling between the vehicle and guideway is weak or when vehicle speed is below certain values (11-13).

The focus of our study is the steady-state or repetitive condition of guideway deflections and vehicle heave accelerations for the vehicles with a vertical motion. The steady state exists after a vehicle with a given arbitrary set of initial conditions has traversed a sufficient number of spans in which the state of the vehicle entering a span is identical to its state when leaving the span or, in fact, entering the next span. For a vehicle starting under zero initial conditions, the number of spans a vehicle must cross to reach a steady-state condition depends on the number of modes and traveling-speed ratio of the vehicle. The maximum number of spans a vehicle must cross to reach a steady state is <100, in accordance with calculated results (11-13).

Table 1 shows the vehicle and guideway parameters we used in our simulation for the maglev systems shown in Figs. 1 and 2.

Two-Degree-of-Freedom Vehicle

If we set M = 1 and N = 1 in Eqs. 11 and 12, the vehicle appears to be a two-degree-of-freedom model that provides a relatively simple explanation of the dynamic behavior of vehicle/guideway systems (11,12).

Figure 3 shows the maximum guideway displacement ratio Y_g ($= y_g/y_m$) and maximum vehicle acceleration ratios $\ddot{Y}_p$ ($= \ddot{y}_p/y_m$) and $\ddot{Y}_s$ ($= \ddot{y}_s/y_m$) for both primary and secondary suspensions as a function of vehicle-traveling-speed ratio v/v_c on both single- and double-span guideways. v_c is the first critical speed $\left[=(\pi/L)(\sqrt{EI/m})\right]$. For a single-span beam, the peak of maximum displacement ratio is ≈1.7 when v/v_c is ≈0.6 for an uncoupling model, while for a coupling model the peak of maximum displacement declines to 1.5 when v/v_c is ≈0.4. When v/v_c is <0.4, the coupled and uncoupled modes remain in good agreement. Therefore, for low values of v/v_c, an uncoupling model may be sufficient to simulate dynamics of vehicle/guideway systems, i.e., dynamic motions of the vehicle and guideway can be decoupled, the vehicle may be considered a moving force on the guideway, and guideway deflection is then used as a known displacement input into the suspensions. For the double-span guideway, when the vehicle-traveling-speed ratio $v/v_c < 0.5$, the maximum displacement ratios at both $\xi = 0.5$ and $\xi = 1.5$ ($\xi = x/L$) are much smaller than those of the single-span guideway. The differences between uncoupling and coupling models for the double-span guideway are smaller than those of the single-span guideway. From comparisons of vehicle accelerations, the amplitudes of maximum accelerations of both primary and secondary suspensions for the double-span guideway are lower than those of the single-span guideway. Because v/v_c in maglev systems is expected to be no higher than 0.5 (9), and without considering other factors, a two-span beam appears to be more efficient in achieving better ride quality.

More-detailed parameter analyses for the two-degree-of-freedom vehicle model can be found in Ref. 11.

Effects of Distributed Loads

For a dynamic analysis of vehicle/guideway interactions, an understanding of the effects of distributed loads is essential. In a single-car vehicle (system parameters are given in Table 1) as shown in Fig. 2, for any given span configuration, span deflections decrease as the number of magnets is increased and total force is held constant. These effects exist when the vehicle travels at certain speeds. Figure 4 shows the midspan deflections of a single-span beam when a single-car vehicle, which has one, two, four, and eight magnets attached, travels at 100 m/s (360 km/h). Figure 5 shows the maximum midspan deflections as a function of vehicle traveling velocity. Apparently, the one-magnet case, which represents a two-degree-of-freedom vehicle with a concentrated load, causes the largest beam deflection. The responses of four magnets and eight magnets have almost the same order deflections when the traveling velocity is greater than 50 m/s (180 km/h).

Table 1. Parameters for dynamic interaction analysis of maglev systems

Vehicle	
Vehicle length ℓ	25.0 m
Magnet mass m_p	1016 kg
Car-body mass m_s	45700 kg
Primary damping c_p	3.45×10^4 N-s/m
Secondary damping c_s	2.15×10^4 N-s/m
Primary stiffness k_p	1.45×10^4 N/m
Secondary stiffness k_s	2.26×10^4 N/m
Intercar vertical stiffness k_v	2.26×10^4 N/m
Intercar vertical damping c_v	0.0
Guideway	
Length of span L	25.0 m
Bending rigidity EI	7.16×10^9 N-m^2
Mass per unit length m	1.82×10^3 kg/m
Damping ζ_n	3%

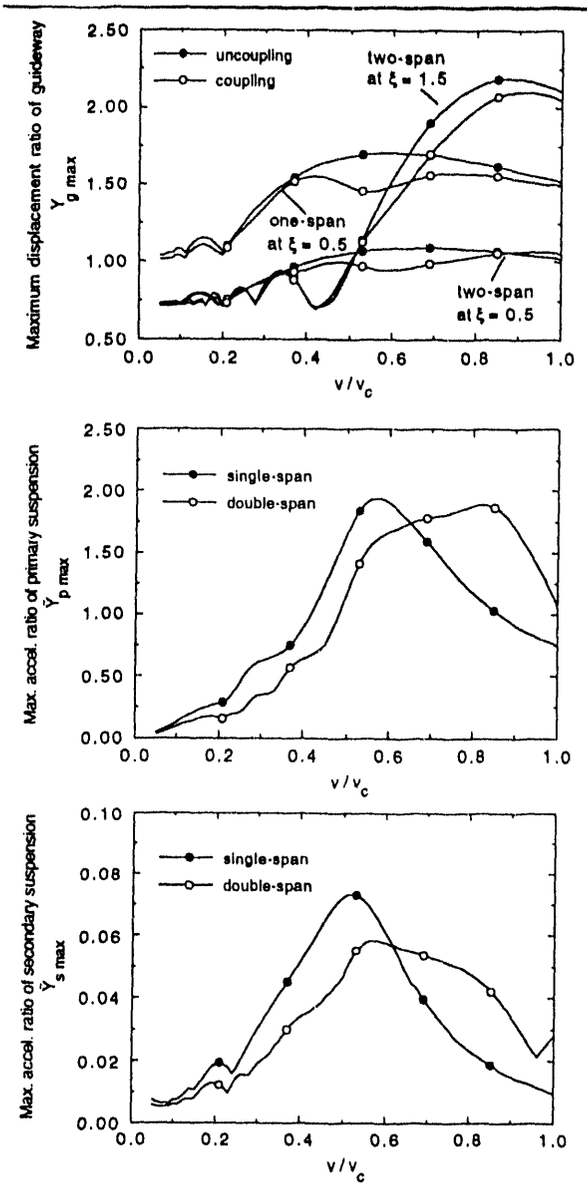

Fig. 3 Effects of single-span and double-span beams on maximum guideway displacement and vehicle acceleration ratios for two-degree-of-freedom vehicle

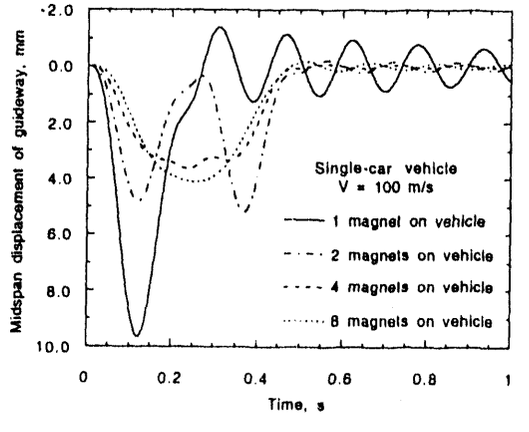

Fig. 4 Midspan displacement of guideway for single car with various magnets traveling along guideway at 100 m/s (360 km/h)

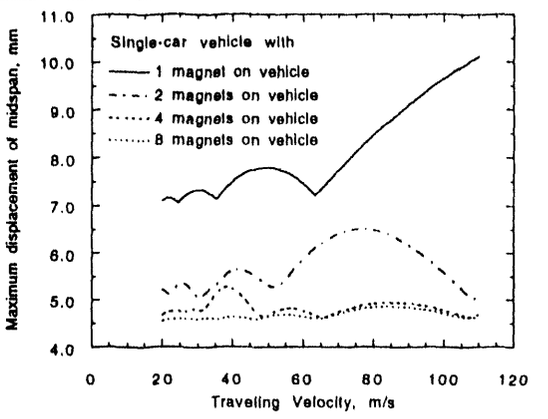

Fig. 5 Maximum midspan displacements of guideway for single car with various magnets traveling along guideway at various speeds

Dynamics of Multicar Vehicle

Multicar-vehicle dynamics are simulated with the model in Fig. 1.

Figure 6 shows midspan beam deflections when multicar vehicles (1, 2, 3, and 4 cars) travel at 100 m/s. No matter how many cars are included in the vehicle, the maximum beam deflection remains the same. But the duration of deflections increases as car number increases.

Figure 7 shows car body accelerations for vehicles with various cars when traveling speed is 100 m/s (360 km/h). We note that the single-car vehicle has the largest peak-to-peak acceleration and that the multicar-vehicle peak-to-peak acceleration decreases, which indicates that intercar restraints affect vehicle motions and that the multicar vehicles may have better ride comfort.

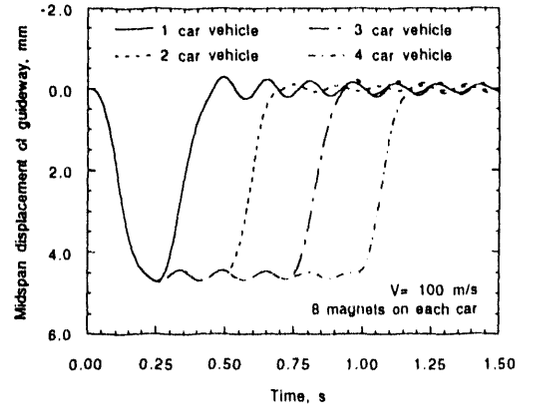

Fig. 6 Midspan displacements of guideway for multicar vehicles with eight magnets on each car traveling along guideway at 100 m/s (360 km/h)

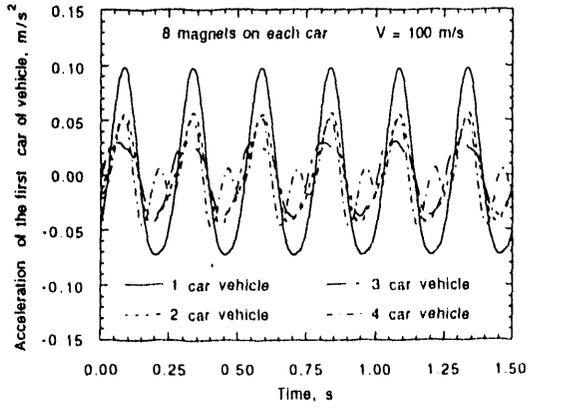

Fig. 7 Car body accelerations for multicar vehicles with eight magnets on each car traveling along guideway at 100 m/s (360 km/h)

Ride Comfort of Multicar Vehicle

Figure 8 shows power spectral densities (PSDs) of car body accelerations for multicar vehicles traveling at 100 m/s. For comparison, the Urban Tracked Air Cushion Vehicle (UTACV) ride comfort criterion (ranging from 0-10 Hz) is also shown. Based on the parameters in Table 1, the PSDs satisfy the ride comfort criterion. It appears that the vehicle with those parameters can provide an acceptable ride. From Fig. 8, we also note that at the fundamental frequency, the PSDs of acceleration decrease as car number increases; however, at higher harmonic frequencies, this tendency is less clear.

Figure 9 shows PSDs of acceleration of a two-car vehicle traveling at various speeds; the harmonic frequencies vary with traveling speed.

CLOSING REMARKS

(1) This study developed a dynamic interaction model of a maglev system with a multicar, multiload vehicle traveling along a flexible guideway. This model is desirable for analyses of vehicle/guideway interactions in maglev systems. The model can be incorporated into future computer codes for nonlinear dynamic analyses of maglev systems; it has already been incorporated into a computer code (to be published) at Argonne National Laboratory that contains a six-degree-of-freedom rigid-vehicle body. The model should have a bright future with many applications in commercial maglev systems.

(2) A distributed-load vehicle model is better than a concentrated-load model that may result in large amplitudes of both guideway deflections and vehicle accelerations in simulations. Multicar vehicles have less car-body acceleration than does a single-car vehicle, because of intercar constraints. This indicates that the multicar vehicle would provide better ride comfort.

(3) Maglev systems may become a major transportation mode in the 21st century. Because the cost for a commercial maglev system is still very high, it is wise to consider dynamic control systems before completing the guideway design so that overall system cost can be reduced.

ACKNOWLEDGMENTS

This work was performed under the sponsorship of the U.S. Army Corps of Engineers and the Federal Railroad Administration through inter-agency agreements with the U.S. Department of Energy.

REFERENCES

(1) Bohn, G., and Steinmetz, G., Proc. Int. Conf. Maglev Transport '85, Sept. 17-19, 1985, Keidanren Kaikan, Tokyo, Japan, Publ. by IEEE, Japan, pp. 107-114, 1985.

(2) Chen, S. S., Rote, D. M., and Coffey, H. T., A Review of Vehicle/Guideway Interactions in Maglev Systems, ASME Publication, PVP-Vol. 231, pp. 81-95, 1992.

(3) Coffey, H. T., et al., "Preliminary Design for a Maglev Development Facility," Report ANL/ESD-14, Argonne National Laboratory, 1991.

(4) Johnson, L. R., et al., "Maglev Vehicles and Superconductor Technology: Integration of High-Speed Ground Transportation into the Air Travel System," Report ANL/CNSV-67, Argonne National Laboratory, 1989.

(5) Katz, R. M., Nene, V. D., Ravera, R. J., and Skalski, C. A., ASME Trans., J. Dynamic Systems, Measurement, and Control, Vol. 96, pp. 204-212, 1974.

(6) Zicha, J. H., Int. Conf. Maglev and Linear Drives, Publication IEEE 86CH2276, pp. 69-87, 1986.

(7) Chiu, W. S., Smith, R. G., and Wormley, D. N., ASME Trans., J. Dynamic Systems, Measurement, and Control, pp. 25-34, 1971.

(8) Iguchi, M , and Hara, H., Proc. Int. Conf. Maglev Transport '85, Sept. 17-19, 1985, Keidanren Kaikan, Tokyo, Japan, Publ. by IEEE, Japan, pp. 217-224, 1985.

(9) Sinha, P. K., Electromagnetic Suspension, Dynamics and Control, Peter Peregrinus Ltd., London, U.K., 1987.

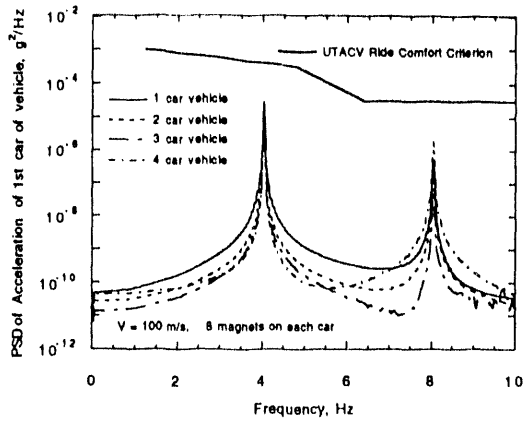

Fig. 8 PSD values of car-body accelerations for multicar vehicles with eight magnets on each car traveling along guideway at 100 m/s; UTACV Ride Comfort Criterion shown for comparison

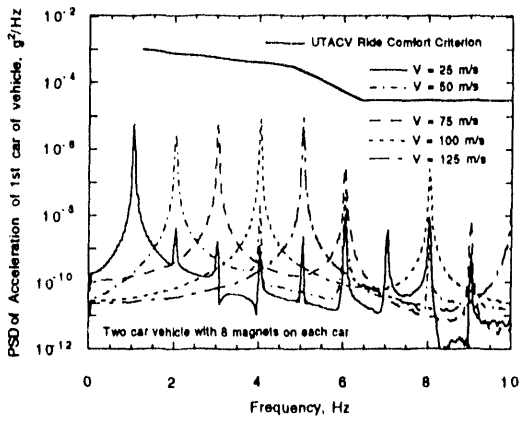

Fig. 9 PSD values of car-body accelerations for two-car vehicle with eight magnets on each car traveling along guideway at various speeds; UTACV Ride Comfort Criterion shown for comparison

(10) Uher, R. A., Proc. Int. Conf. Maglev '89, July 1989, pp. 115-122, 1989.

(11) Cai, Y., Chen, S. S., and Rote, D. M., "Vehicle/Guideway Interaction in Maglev Systems," Report ANL-92/19, Argonne National Laboratory, 1992.

(12) Cai, Y., Chen, S. S., Rote, D. M., and Coffey, H. T., Proc. CSME Forum 1992 "Transport 1992+," June 1-4, 1992, Montreal, Canada, Vol. III, pp. 750-757, 1992.

(13) Cai, Y., Chen, S. S., and Rote, D. M., "Dynamics and Controls in Maglev Systems," Report ANL-92/43, Argonne National Laboratory, 1992.

(14) Cai, Y., Chen, S. S., Zhu, S., Mulcahy, T. M., Rote, D. M., and Coffey, H. T., Proc. Maglev '93, 13th Int. Conf. on Magnetically Levitated Systems and Linear Drivers, May 19-21, 1993, Argonne, IL, USA, pp. 265-270, 1993.

(15) Vu-Quoc, L., and Olsson, M., ASME Trans., J. Applied Mechanics, Vol. 56, pp. 451-458, 1989.

(16) Richardson, H. H., and Wormley, D. N., ASME Trans., J. Dynamic Systems, Measurement, and Control, Vol. 96, pp. 169-179, 1974.

DATE
FILMED
12/01/93
END